Available online at www.sciencedirect.com
SCIENCE DIRECT®
International Journal of Thermal Sciences 44 (2005) 809–821
International Journal of Thermal Sciences
www.elsevier.com/locate/ijts

Fundamentals of a new method for the solution of the radiative transfer equation ☆

P.J. Coelho *

Mechanical Engineering Department, Instituto Superior Técnico, Technical University of Lisbon, Av. Rovisco Pais, 1049-001 Lisboa, Portugal

Received 4 August 2004; received in revised form 13 February 2005; accepted 14 February 2005

Available online 7 April 2005

Abstract

The fundamentals of a new radiation model are described in this paper. The spatial and angular dependence of the radiation intensity are split in such a way that the radiation intensity is approximated by a linear combination of basis functions dependent only on the angular direction. The coefficients of the approximation are functions of the spatial coordinates. The spatial discretization is performed using the finite volume method and the angular discretization is based on the finite element method. This means that the basis functions are defined according to the criteria used in the finite element method. The step scheme was employed in the spatial discretization and bilinear basis functions were chosen for the angular discretization. The method may be applied to both grey and non-grey media, non-scattering and scattering media, simple and complex geometries. However, it is still in an early stage of development, and therefore it is applied in this paper to simple one-dimensional problems of radiative transfer in enclosures with grey, emitting-absorbing and scattering media. The results obtained show that the method gives good results for several benchmark problems with available analytical solutions, and converges to the exact solution as the grid is refined and the number of terms in the approximation increases.

Keywords: Radiative transfer equation; Finite volume method; Finite element method; Hybrid method; Spatial discretization; Angular discretization

1. Introduction

Radiative heat transfer plays an important role in many engineering problems because of the need to predict or measure heat transfer in furnaces, boilers, engines and rocket nozzles. It is also relevant to many industrial heating, cooling and drying processes, as well as to solar radiation. In most problems of practical relevance, radiation propagates throughout a medium that absorbs, emits, and often scatters radiation. Several methods have been developed to compute radiative heat transfer in participating media. These include, among others, the zonal [1], Monte Carlo [2], spherical harmonics [3], YIX [4], discrete transfer [5], discrete ordinates [6] and finite volume [7] methods. All these methods have their merits and shortcomings, and no one is considered as the best one for all applications.

The zonal method was originally developed for rectangular enclosures and non-scattering or isotropically scattering media. Later developments have allowed the relaxing of these restrictions. Nevertheless, the calculation of exchange areas in geometrically complex enclosures is a challenging issue, and the computational requirements are high. The Monte Carlo method can be used to address very complex problems, either in terms of geometry or radiative properties of the medium and boundary surfaces. However, it is also very time consuming, even for relatively simple problems, and therefore other less computationally demanding methods are often preferred. The spherical harmonics method has a sound mathematical foundation, but it is only competitive if a low order approximation is employed. The P1 approximation is very popular, but it is often inaccurate

☆ A preliminary version of this paper was presented at CHT-04: An ICHMT International Symposium on Advances in Computational Heat Transfer, April 2004, G. de Vahl Davis and E. Leonardi (Eds.), CD-ROM Proceedings, ISBN 1-5670-174-2, Begell House, New York, 2004.

* Fax: +351 21 8475545; phone: +351 21 8418194.
E-mail address: coelho@navier.ist.utl.pt (P.J. Coelho).

1290-0729/$ – see front matter
doi:10.1016/j.ijthermalsci.2005.02.008

Nomenclature

A_1	coefficient of a linearly anisotropic phase function	**r**	position vector ..... m
E	number of control angle elements; absolute error	**s**	unit vector along the direction of propagation of radiation
G	incident radiation ..... $\mathrm{W\cdot m^{-2}}$	x	coordinate along the direction normal to the wall ..... m
I_b	blackbody radiation intensity .... $\mathrm{W\cdot m^{-2}\cdot sr^{-1}}$	Δx	Length of a control volume ..... m
L	distance between the walls ..... m	*Greek symbols*	
n	outer unit vector normal to the wall	η	relative error
N	total number of angular nodes	μ	direction cosine of the x direction
N_e	number of angular nodes in a control angle element	μ_k	direction cosine of the kth direction
N_x	number of spatial control volumes	ϕ	basis function
N_θ	number of polar angles per octant	ψ	shape function
N_φ	number of azimuthal angles per octant		
q_w	incident heat flux on the wall ..... $\mathrm{W\cdot m^{-2}}$		

for strongly anisotropic media, while the P3 approximation is mathematically involved and does not significantly improve the results. The YIX is based on the solution of the integral form of the radiative transfer equation along prescribed directions. It is an efficient solution method compared with other methods for the solution of the integral form of the radiative transfer equation, and can be applied to nonhomogeneous and non-grey media. However, it suffers from ray effects. The discrete transfer method is relatively accurate, flexible and economical from the computational point of view. However, the calculation of the divergence of the radiative heat flux, which constitutes the radiative heat source of the energy equation, may require a very fine angular discretization to achieve accurate results. Moreover, the method is not applicable to anisotropic scattering media.

The discrete ordinates and the finite volume method have received significant attention and development in the last decade due to their good compromise between accuracy, computational economy and flexibility. Moreover, they are easily coupled with computational fluid dynamics codes. However, these methods also have their limitations. The two most important ones are ray effects and false scattering [8]. Ray effects are a consequence of the angular discretization and result from the representation of the continuously varying angular distribution of the radiation intensity by a discrete set of solid angles spanning the whole space, such that the radiation intensity is assumed to be constant within each solid angle. False scattering is a consequence of the spatial discretization and results from the diffusive nature of many spatial discretization schemes.

Significant efforts have been directed to reduce the impact of the errors mentioned above. False scattering may be significantly reduced using bounded high order resolution schemes formerly developed for computational fluid dynamics [9]. As far as ray effects are concerned, more accurate quadratures and angular discretizations have been proposed [10], but they are unable to significantly reduce ray effects. The modified discrete ordinates and finite volume methods [11–13] successfully mitigate ray effects caused by discontinuities or sharp gradients of the temperature of the boundaries, but they are ineffective if ray effects are due to sharp gradients of the temperature of the medium. A new modified version has been proposed in [14], which also mitigates ray effects originated from sharp gradients of the temperature of the medium. However, this method is more time consuming, and becomes prohibitively expensive in the case of anisotropic scattering.

In this paper, the fundamentals of a new method for the solution of the radiative transfer equation are described, and the method is applied to one-dimensional problems in grey media. The method relies on a finite element approximation to the angular dependence of the radiation intensity. Therefore, the discrete angular discretization employed in the discrete ordinates and finite volume methods is avoided, and it is expected that this may alleviate ray effects, although this issue is not addressed in the present work. The spatial discretization is carried out using a finite volume method. The method will be referred to as HYDRA, which stands for HYbrid finite volume/finite element Discretization method for the solution of the RAdiative transfer equation, or in short, HYbrid Discretization for RAdiation. A finite element formulation of the discrete ordinates method was used in [15]. However, the method developed in [15] is completely different from that proposed here. In that work, the finite element method was used in the spatial discretization to enable the solution of complex geometry problems. Here, the spatial discretization is carried out using the finite volume method, and the finite element approximation is used for the angular discretization. The finite element method has also been used to solve radiation problems [16] but using the integral formulation of the radiative transfer equation.

2. Radiation model

The radiative heat transfer equation for a grey medium may be written as

$$\mathbf{s}\cdot\nabla I(\mathbf{r},\mathbf{s}) = -\beta I(\mathbf{r},\mathbf{s}) + \kappa I_b(\mathbf{r}) + \frac{\sigma_s}{4\pi}\int_{4\pi} I(\mathbf{r},\mathbf{s}')\Phi(\mathbf{s}',\mathbf{s})\,\mathrm{d}\Omega' \tag{1}$$

Although the present method can be applied to non-grey media, only grey media are considered in this work, and therefore the wavelength dependence of the radiation intensity and radiative properties is omitted. In one-dimensional media, this equation takes the following form

$$\mu(\mathbf{s})\frac{\partial I(\mathbf{r},\mathbf{s})}{\partial x} = -\beta I(\mathbf{r},\mathbf{s}) + \kappa I_b(\mathbf{r}) + \frac{\sigma_s}{4\pi}\int_{4\pi} I(\mathbf{r},\mathbf{s}')\Phi(\mathbf{s}',\mathbf{s})\,\mathrm{d}\Omega' \tag{2}$$

The boundary condition for a diffuse surface is given by

$$I(\mathbf{r}_w,\mathbf{s}) = \varepsilon I_b(\mathbf{r}_w) + \frac{\rho}{\pi}\int_{\mathbf{n}\cdot\mathbf{s}'<0} I(\mathbf{r}_w,\mathbf{s}')|\mathbf{n}\cdot\mathbf{s}'|\,\mathrm{d}\Omega' \tag{3}$$

The radiation intensity is approximated by splitting the spatial and angular dependence as follows

$$I(\mathbf{r},\mathbf{s}) = \sum_{m=1}^{N} I^m(\mathbf{r})\phi_m(\mathbf{s}) \tag{4}$$

Here, $\phi_m(\mathbf{s})$ are linearly independent functions that constitute the basis of a space of rank N. In the present method, these functions are prescribed according to the finite element method, as described below. They are a function of the $\mathbf{s}$ direction, and therefore a function of the polar and azimuthal angles. $I^m(\mathbf{r})$ are unknown functions that depend only on the spatial coordinates from which the radiation intensity field $I(\mathbf{r},\mathbf{s})$ may be defined. Inserting Eq. (4) into Eq. (2) yields

$$\mu(\mathbf{s})\left(\sum_{m=1}^{N}\phi_m(\mathbf{s})\frac{\partial I^m(\mathbf{r})}{\partial x}\right) = -\beta\sum_{m=1}^{N} I^m(\mathbf{r})\phi_m(\mathbf{s}) + \kappa I_b(\mathbf{r}) + \frac{\sigma_s}{4\pi}\sum_{l=1}^{N} I^l(\mathbf{r})\int_{4\pi}\phi_l(\mathbf{s}')\Phi(\mathbf{s}',\mathbf{s})\,\mathrm{d}\Omega' \tag{5}$$

Now, both terms of this equation are multiplied by the nth basis function and integrated over all directions:

$$\int_{4\pi}\mu(\mathbf{s})\left(\sum_{m=1}^{N}\phi_m(\mathbf{s})\frac{\partial I^m(\mathbf{r})}{\partial x}\right)\phi_n(\mathbf{s})\,\mathrm{d}\Omega = -\beta\sum_{m=1}^{N} I^m(\mathbf{r})\int_{4\pi}\phi_m(\mathbf{s})\phi_n(\mathbf{s})\,\mathrm{d}\Omega + \kappa I_b(\mathbf{r})\int_{4\pi}\phi_n(\mathbf{s})\,\mathrm{d}\Omega + \frac{\sigma_s}{4\pi}\sum_{l=1}^{N} I^l(\mathbf{r})\int_{4\pi}\int_{4\pi}\phi_l(\mathbf{s}')\Phi(\mathbf{s}',\mathbf{s})\,\mathrm{d}\Omega'\phi_n(\mathbf{s})\,\mathrm{d}\Omega \quad n=1,2,\ldots,N \tag{6}$$

Since n may change from 1 to N, a set of N simultaneous equations was derived, which allows the calculation of the N unknowns, namely the functions $I^m(\mathbf{r})$. Eq. (6) may be written in a more compact form as

$$\sum_{m=1}^{N}\frac{\mu(\mathbf{s})}{|\mu(\mathbf{s})|}\frac{\partial I^m(\mathbf{r})}{\partial x}A_{mn} = -\beta\sum_{m=1}^{N} I^m(\mathbf{r})B_{mn} + \kappa I_b(\mathbf{r})C_n + \frac{\sigma_s}{4\pi}\sum_{l=1}^{N} I^l(\mathbf{r})D_{ln} \quad n=1,2,\ldots,N \tag{7}$$

Matrices **A**, **B**, **D** and vector **C** have been introduced for conciseness. Their components may be easily obtained from comparison of Eqs. (6) and (7) yielding

$$A_{mn} = \int_{4\pi}|\mu(\mathbf{s})|\phi_m(\mathbf{s})\phi_n(\mathbf{s})\,\mathrm{d}\Omega \tag{8}$$

$$B_{mn} = \int_{4\pi}\phi_m(\mathbf{s})\phi_n(\mathbf{s})\,\mathrm{d}\Omega \tag{9}$$

$$C_n = \int_{4\pi}\phi_n(\mathbf{s})\,\mathrm{d}\Omega \tag{10}$$

$$D_{mn} = \int_{4\pi}\int_{4\pi}\phi_m(\mathbf{s}')\Phi(\mathbf{s}',\mathbf{s})\,\mathrm{d}\Omega'\phi_n(\mathbf{s})\,\mathrm{d}\Omega \tag{11}$$

If the medium scatters isotropically, then the scattering phase function is equal to 1 and matrix **D** is evaluated as

$$D_{mn} = \int_{4\pi}\int_{4\pi}\phi_m(\mathbf{s}')\,\mathrm{d}\Omega'\phi_n(\mathbf{s})\,\mathrm{d}\Omega = \int_{4\pi}\phi_n(\mathbf{s})\,\mathrm{d}\Omega\int_{4\pi}\phi_m(\mathbf{s}')\,\mathrm{d}\Omega' = C_mC_n \tag{12}$$

In the case of a linearly anisotropic medium, the phase function is given by

$$\Phi(\mathbf{s}',\mathbf{s}) = 1 + A_1\mathbf{s}\cdot\mathbf{s}' = 1 + A_1\sum_{k=1}^{3}\mu_k\mu_k' \tag{13}$$

where A_1 is a constant. The subscript k was omitted formerly because we are dealing with one-dimensional media, but must be retained here. Therefore, $\mu\equiv\mu_1$. Inserting Eq. (13) into Eq. (11) yields

$$D_{mn} = \int_{4\pi}\int_{4\pi} \phi_m(\mathbf{s}')\left(1 + A_1\sum_{k=1}^{K}\mu_k\mu_k'\right)\mathrm{d}\Omega'\phi_n(\mathbf{s})\,\mathrm{d}\Omega$$
$$= \int_{4\pi}\phi_n(\mathbf{s})\,\mathrm{d}\Omega\int_{4\pi}\phi_m(\mathbf{s}')\,\mathrm{d}\Omega'$$
$$+ A_1\sum_{k=1}^{3}\left(\int_{4\pi}\mu_k\phi_n(\mathbf{s})\,\mathrm{d}\Omega\int_{4\pi}\mu_k'\phi_m(\mathbf{s}')\,\mathrm{d}\Omega'\right)$$
$$= C_mC_n + A_1\sum_{k=1}^{3}E_{m,k}E_{n,k} \tag{14}$$

where

$$E_{m,k} = \int_{4\pi}\mu_k\phi_m(\mathbf{s})\,\mathrm{d}\Omega \tag{15}$$

Complicated phase functions are often approximated by simpler ones, such as the delta-Eddington phase function [17], where the forward scattering peak typically observed for large particles is separated from the rest of the scattering phase function:

$$\delta(\mathbf{s},\mathbf{s}') = 2f\delta[1-\mathbf{s}\cdot\mathbf{s}'] + (1-f)[1+3g\mathbf{s}\cdot\mathbf{s}'] \tag{16}$$

where f is the forward scattering factor and g the asymmetry factor.

In this case, the in-scattering term takes the following form

$$\frac{\sigma_s}{4\pi}\int_{4\pi} I(\mathbf{r},\mathbf{s}')\Phi(\mathbf{s}',\mathbf{s})\,\mathrm{d}\Omega'$$
$$= \sigma_s f I(\mathbf{r},\mathbf{s}) + \frac{1-f}{4\pi}\sigma_s\int_{4\pi} I(\mathbf{r},\mathbf{s}')[1+3g\mathbf{s}\cdot\mathbf{s}']\,\mathrm{d}\Omega' \tag{17}$$

The first term on the right of Eq. (17) is added to the out-scattering term, while the second term is handled as explained above for a linearly anisotropic scattering phase function.

Eq. (7) has been discretized in the angular domain, but the spatial discretization has not yet been carried out. Different methods may be used for this purpose, but here we will use the finite volume method, which is particularly convenient in the case of coupled CFD/heat transfer problems for compatibility reasons, since the finite volume method is widely used in CFD. Spatial discretization requires the approximation of the first derivative on the left side of Eq. (7) in terms of the radiation intensity at the grid nodes. The term to be discretized is similar to the convective term in the momentum equations. It is well known from CFD that the discretization of the convective term is a challenging task, and many discretization methods have been proposed. In the radiation community, the step scheme is often employed. This scheme is the counterpart of the upwind scheme in CFD, which is widely recognized to be unsatisfactory due to false diffusion. More accurate schemes are available and should be employed. Moreover, they can be employed to discretize Eq. (7). However, in the present work we are focused on the development of a new solution method for the radiative transfer equation, and therefore we wish to avoid any complexities arising from the spatial discretization. Accordingly, we will simply use the step scheme, although realizing that more accurate schemes should be preferred, and could be employed.

The right side of Eq. (7) is assumed to be constant within a control volume. Therefore, integrating Eq. (7) over a control volume of length Δx and applying the step scheme gives

$$\sum_{m=1}^{N}\left(I_{\mathrm{out}}^m - I_{\mathrm{in}}^m\right)A_{mn}$$
$$= -\beta\Delta x\sum_{m=1}^{N}I_P^m B_{mn} + \kappa\Delta x I_{b,P}C_n + \frac{\sigma_s}{4\pi}\Delta x\sum_{l=1}^{N}I_P^l D_{\ln}$$
$$n = 1,2,\ldots,N \tag{18}$$

where I_{in}^m and I_{out}^m are the mth coefficient of the radiation intensity entering and leaving the control volume. Since the step scheme yields $I_{\mathrm{out}}^m = I_P^m$, Eq. (18) may be rearranged as

$$\sum_{m=1}^{N}(A_{mn} + \beta\Delta x B_{mn})I_P^m$$
$$= \sum_{m=1}^{N}I_{\mathrm{in}}^m A_{mn} + \kappa\Delta x I_{b,P}C_n + \frac{\sigma_s}{4\pi}\Delta x\sum_{l=1}^{N}I_P^l D_{\ln}$$
$$n = 1,2,\ldots,N \tag{19}$$

This completes the discretization task, and the solution of the set of $N_x \times N$ equations (19), where N_x stands for the number of spatial control volumes, gives the numerical solution of the radiative transfer equation. However, neither the basis functions were defined nor the solution method has been outlined. These issues are addressed below.

The basis functions are defined according to finite element criteria. This means that the N values appearing in Eq. (4), which are defined over a spherical surface, may be interpreted as nodes that define a grid. These nodes will be referred to as angular nodes, and the elements by control angle elements. Here, bilinear elements are chosen, and the grid is defined in such a way that either the polar or the azimuthal angle remains constant along the boundaries of the elements, as shown in Fig. 1. This means that a classical polar/azimuthal discretization is carried out, like in the finite volume and discrete transfer methods. However, while in these methods the radiation intensity is constant over a control angle or a solid angle, respectively, in the present method the radiation intensity is a continuously varying function, because the basis functions vary continuously within the control angle elements.

The mth basis function is equal to 1 at node m and equal to zero at all the other nodes. This function is identically equal to zero for all but the elements that are connected to

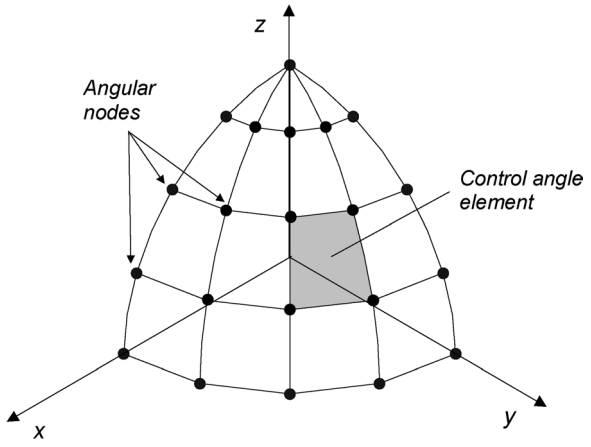

Fig. 1. Control angle elements.

node m. The restriction of a basis function to a control angle element is referred to as shape function, as in the finite element terminology, and is denoted by ψ.

Let Ω_e be a control angle element such that $\theta_i \leqslant \theta \leqslant \theta_{i+1}$ and $\varphi_j \leqslant \varphi \leqslant \varphi_{j+1}$. There are only 4 basis functions that are different from zero in this element, which are the basis functions that take the value 1 at one of the nodes of the element and the value 0 at the three other nodes. The 4 shape functions of this element are defined as

$$\psi_1^e(\theta,\varphi) = \frac{\theta-\theta_i}{\theta_{i+1}-\theta_i}\frac{\varphi-\varphi_j}{\varphi_{j+1}-\varphi_j} \tag{20}$$

$$\psi_2^e(\theta,\varphi) = \frac{\theta-\theta_{i+1}}{\theta_i-\theta_{i+1}}\frac{\varphi-\varphi_j}{\varphi_{j+1}-\varphi_j} \tag{21}$$

$$\psi_3^e(\theta,\varphi) = \frac{\theta-\theta_{i+1}}{\theta_i-\theta_{i+1}}\frac{\varphi-\varphi_{j+1}}{\varphi_j-\varphi_{j+1}} \tag{22}$$

$$\psi_4^e(\theta,\varphi) = \frac{\theta-\theta_i}{\theta_{i+1}-\theta_i}\frac{\varphi-\varphi_{j+1}}{\varphi_j-\varphi_{j+1}} \tag{23}$$

The radiation intensity over an element may be expressed as a linear combination of the shape functions of that element as

$$I^e(\mathbf{r},\mathbf{s}) = \sum_{m=1}^{N_e} I^{m,e}(\mathbf{r})\psi_m^e(\mathbf{s}) \tag{24}$$

where the superscript m, e denotes the mth angular node of the eth control angle element, and N_e is the number of angular nodes in a control angle element, which is equal to 4 in the case of bilinear elements. The relation between the N angular nodes of the 4π angular domain and the N_e angular nodes of every control angle element is stored in a mapping matrix. Eq. (19) may be written for element Ω_e as

$$\begin{aligned}&\sum_{m=1}^{N_e}\left(a_{mn}^e + \beta\Delta x b_{mn}^e\right) I_P^{m,e} \\ &\quad = \sum_{m=1}^{N_e} I_{\text{in}}^{m,e} a_{mn}^e + \kappa\Delta x I_{b,P} c_n^e + \frac{\sigma_s}{4\pi}\Delta x \sum_{l=1}^{N_e} I_P^{l,e} d_{\text{ln}}^e \\ &\quad n = 1,2,\ldots,N_e\end{aligned} \tag{25}$$

where a_{mn}^e, b_{mn}^e, c_n^e and d_{mn}^e are the components of local element matrices (vector, in the case of c_n^e) of rank 4 for bilinear shape functions defined over the domain of a control angle element. Therefore, the components of global matrices **A**, **B**, **D**, **E** and global vector **C** are not calculated directly over the whole angular domain using Eqs. (8)–(11) and Eq. (15). Instead, they are calculated element by element, like the stiffness and load matrices in the finite element method, using the shape functions defined above.

The components of the local element matrices are defined as

$$a_{mn}^e = \int_{\Omega_e} \left|\mu(\mathbf{s})\right| \psi_m^e(\mathbf{s})\psi_n^e(\mathbf{s})\,\mathrm{d}\Omega_e \tag{26}$$

$$b_{mn}^e = \int_{\Omega_e} \psi_m^e(\mathbf{s})\psi_n^e(\mathbf{s})\,\mathrm{d}\Omega_e \tag{27}$$

$$c_n^e = \int_{\Omega_e} \psi_n^e(\mathbf{s})\,\mathrm{d}\Omega_e \tag{28}$$

$$d_{mn}^e = \int_{\Omega_e}\int_{\Omega_e'} \psi_m^e(\mathbf{s}')\Phi(\mathbf{s}',\mathbf{s})\,\mathrm{d}\Omega_e'\psi_n^e(\mathbf{s})\,\mathrm{d}\Omega_e \tag{29}$$

$$e_{m,k}^e = \int_{\Omega_e} \mu_k \psi_m^e(\mathbf{s})\,\mathrm{d}\Omega_e \tag{30}$$

The components of these matrices are calculated analytically for every control angle element. The only exception is matrix $\mathbf{d}^e$, whose components may require numerical integration, depending on the scattering phase function. In the case of isotropic or linear anisotropic scattering, analytical integration is possible, yielding

$$d_{mn}^e = c_m^e c_n^e \tag{31}$$

for isotropic scattering and

$$d_{mn}^e = c_m^e c_n^e + A_1 \sum_{k=1}^{3} e_{m,k}^e e_{n,k}^e \tag{32}$$

for linear anisotropic scattering. In the case of a delta–Eddington phase-function, analytical integration is also possible, since the last term on the right side of Eq. (17) is identical to the in-scattering term of a linearly anisotropic scattering phase function, apart from the factor $(1-f)$.

The components of the local element matrices/vector $\mathbf{a}^e$, $\mathbf{b}^e$, $\mathbf{c}^e$, $\mathbf{d}^e$ and $\mathbf{e}^e$ (rank N_e), are transferred to global element matrices/vector $\mathbf{A}^e$, $\mathbf{B}^e$, $\mathbf{C}^e$, $\mathbf{D}^e$ and $\mathbf{E}^e$ (rank N). The components of the global element matrices are easily obtained from the components of the local element matrices using the mapping matrix. The global element matrices are assembled as in the finite element method to obtain the global matrices. Hence, the components of the global matrices are calculated as follows

$$A_{mn} = \sum_{e=1}^{E} A_{mn}^e \tag{33}$$

$$B_{mn} = \sum_{e=1}^{E} B_{mn}^{e} \tag{34}$$

$$C_n = \sum_{e=1}^{E} C_n^e \tag{35}$$

$$D_{mn} = \sum_{e=1}^{E} D_{mn}^{e} \tag{36}$$

$$E_{m,k} = \sum_{e=1}^{E} E_{m,k}^{e} \tag{37}$$

Many different solution methods may be employed to solve the set of $N_x \times N$ equations (19). A simple solution method was employed in this work, which combines an iterative solver with a direct solver. It is likely that other solvers will produce faster convergence, but this requires further investigation.

In the present method, the equations for all the directions become coupled together, in contrast with the discrete ordinates and the finite volume methods. However, the matrix of coefficients is sparse, as a consequence of the use of finite element criteria to select the basis functions, allowing fast solvers to be employed. In this work, the N_x spatial grid nodes are treated sequentially, using the Gauss–Seidel iterative procedure. The set of N equations for the grid node under consideration (Eqs. (19)) is solved using a subroutine from LINPACK [18] suitable for sparse linear sets of equations, assuming that the radiation intensity at the spatial neighbours of the grid node under consideration, i.e., I_{in}^{m}, are known. Therefore, one iteration consists of the solution of N_x sets of N simultaneous equations. The iterative procedure continues until the difference between the incident radiation on the walls in two successive iterations decreases below a prescribed tolerance.

Two quantities of major relevance in radiative transfer problems are the incident radiation and the heat flux. The incident radiation is calculated as

$$G = \int_{4\pi} I(\mathbf{r}, \mathbf{s})\, \mathrm{d}\Omega = \sum_{m=1}^{N} I^{m}(\mathbf{r}) \int_{4\pi} \phi_m(\mathbf{s})\, \mathrm{d}\Omega = \sum_{m=1}^{N} I^{m}(\mathbf{r}) C_m \tag{38}$$

The calculation is performed by assembling the results from all control angle elements as

$$G = \sum_{e=1}^{E} \sum_{m=1}^{N_e} I^{m,e}(\mathbf{r}) c_m^e \tag{39}$$

The incident heat flux on the wall is given by

$$q_w = \int_{2\pi} |\mu| I(\mathbf{r_w}, \mathbf{s})\, \mathrm{d}\Omega = \sum_{\substack{m=1 \\ (\mathbf{s}_m \cdot \mathbf{n} \leqslant 0)}}^{N} I^{m}(\mathbf{r_w}) \int_{2\pi} |\mu| \phi_m(\mathbf{s})\, \mathrm{d}\Omega = \sum_{\substack{m=1 \\ (\mathbf{s}_m \cdot \mathbf{n} \leqslant 0)}}^{N} I^{m}(\mathbf{r_w}) |E_{m,1}| \tag{40}$$

and calculated as

$$q_w = \sum_{e=1}^{E} \sum_{\substack{m=1 \\ (\mathbf{s}_m \cdot \mathbf{n} \leqslant 0)}}^{N_e} I^{m,e}(\mathbf{r}_w) \left| e_{m,1}^{e} \right| \tag{41}$$

Although the method has been described for one-dimensional grey media, the extension to non-grey media and to multidimensional enclosures does not present any major problems. In particular, the development and application to two and three-dimensional enclosures is reported in [19]. The application to geometrically complex enclosures is also feasible, as well as the implementation of more accurate spatial discretization schemes or control angle elements. However, this requires additional work that will constitute the subject of future research. The results described in the following section were obtained using an Alpha processor at 600 MHz. The convergence criterion demands that the difference between two successive iterations of both the incident radiative flux on the boundary and the incident radiation summed over all the spatial control volumes decreases below 10^{-8}.

3. Results and discussion

Calculations were carried out for three one-dimensional radiative transfer problems in Cartesian coordinates. The results are expressed in terms of the radiative flux and divergence of the radiative heat flux. The radiative heat flux for a plane parallel medium is given by [20]:

$$q(\tau) = \int_{4\pi} I(\tau, \theta) \cos\theta\, \mathrm{d}\Omega \tag{42}$$

Here, θ stands for the angle between the normal to the wall and the direction of propagation of radiation and $\tau = \beta x$ is the optical thickness of the medium (see Fig. 2). This expression yields the net heat flux (defined as the difference between the incoming and the outgoing heat flux) at the wall located at $x = L$ if $\tau = \tau_L = \beta L$, and the symmetric of the net heat flux at the wall located at $x = 0$ if $\tau = 0$. If the integration is carried out only for the hemisphere containing the directions pointing towards the wall, then the incident heat flux is obtained rather than the net heat flux. The divergence of the radiative heat flux, which constitutes the radiative heat source of the energy conservation equation, is given by

$$\frac{\mathrm{d}q(\tau)}{\mathrm{d}\tau} = (1 - \omega)(4\pi I_b - G) \tag{43}$$

Emitting-absorbing medium with prescribed temperature. A plane medium that emits and absorbs but does not scatter is taken as the first test problem. The temperature of the medium is 1500 K and the optical thickness has been varied from $\tau_L = 0.1$ to $\tau_L = 10.0$. The temperature of the walls is maintained at 500 K and their emissivity is 0.5. They are treated as diffuse surfaces.

The analytical solution of this problem is given in [20]. Eqs. (42) and (43) take the following form

$$q^*(\tau) = \frac{q(\tau)}{\sigma(T_w^4 - T_{\text{gas}}^4)} = \frac{2[E_3(\tau) - E_3(\tau_L - \tau)]}{1 + (1/\varepsilon - 1)(1 - 2E_3(\tau_L))} \tag{44}$$

$$\frac{\mathrm{d}q^*(\tau)}{\mathrm{d}\tau} = \frac{\mathrm{d}q(\tau)/\mathrm{d}\tau}{\sigma(T_w^4 - T_{\text{gas}}^4)} = -\frac{2[E_2(\tau) + E_2(\tau_L - \tau)]}{1 + (1/\varepsilon - 1)(1 - 2E_3(\tau_L))} \tag{45}$$

where $E_n(x)$ is the exponential integral function of order n, defined as

$$E_n(x) = \int_1^\infty e^{-xt} \frac{\mathrm{d}t}{t^n} \tag{46}$$

Fig. 3 shows the normalized radiative heat source given by Eq. (44) along the distance between the walls for different optical thicknesses ($\tau_L = 0.1$, $\tau_L = 1.0$ and $\tau_L = 10.0$). Only one half of the domain is shown for symmetry reasons. In all cases, the absolute value of the radiative heat source decreases from the walls towards the symmetry plane at $x/L = 0.5$. The radiative heat source is dictated by the contribution of the emission from the medium, which is constant in the case of an isothermal medium, and the incident radiation, as given by Eq. (43). The incident radiation at a given location is due to the radiation intensity that arrives at that location from all the directions, as given by Eq. (38). Let us imagine a case such that the distance between the walls is very large, and consider a point equidistant from the walls. The contribution of the walls to the radiation intensity at that point will be negligible, since the walls are too far away. Only the radiation from the medium will contribute to the incident radiation at that point. The same reasoning may be applied to points in the vicinity of the symmetry plane and far from the walls. This means that the incident radiation will be constant close to the symmetry plane as long as the influence of the walls is negligible.

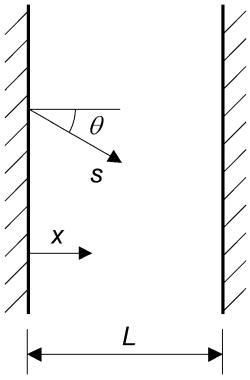

Fig. 2. Radiative transfer in a plane medium between two parallel walls.

At points closer to the wall, the influence of the wall will be visible. In the problem under consideration, the temperature of the wall is lower than the temperature of the medium. Therefore, the radiation intensity leaving the wall is lower than the blackbody radiation intensity at the temperature of the medium. This implies that the incident radiation at a point close to the wall is lower than that at a point far from the wall, and it will decrease as the distance to the wall decreases. Conversely, the absolute value of the radiative heat source increases if the distance from the wall decreases. This behaviour is confirmed by the results displayed in Fig. 3.

In the case of an optically thin medium, the incident radiation is strongly influenced by the radiation intensity leaving the walls, I_w. Moreover, I_w is much lower than I_b in the present problem, and therefore $\mathrm{d}q/\mathrm{d}\tau$ will be approximately constant and large. If, as a rough approximation, G is neglected, then Eq. (43) yields

$$\frac{\mathrm{d}q^*(\tau)}{\mathrm{d}\tau} = \frac{\mathrm{d}q(\tau)/\mathrm{d}\tau}{\sigma(T_w^4 - T_{\text{gas}}^4)} \approx \frac{4T_{\text{gas}}^4}{(T_w^4 - T_{\text{gas}}^4)} = -4.05$$

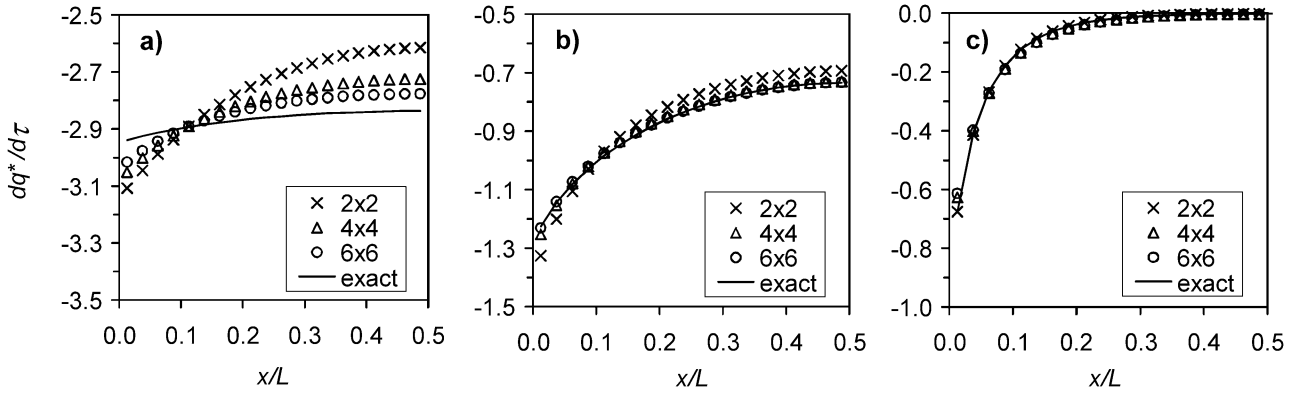

Fig. 3. Normalized radiative heat source (divergence of the radiative heat flux) as a function of the distance between the walls for several angular discretizations. The exact solution is reported in [20]. (a) $\tau_L = 0.1$; (b) $\tau_L = 1.0$; (c) $\tau_L = 10.0$.

Table 1
Root mean square of the radiative heat source normalized by the difference between the emissive power of the medium and the emissive power of the walls. Predictions obtained using the discrete ordinates method (DOM) are also given

Optical thickness	Method		Angular discretization ($N_\theta \times N_\varphi$ per octant)				
			2×2	3×3	4×4	5×5	6×6
0.1	DOM	rms	0.0168	0.0111	0.0080	0.0060	0.0045
	HYDRA	rms	0.0246	0.0182	0.0131	0.0098	0.0075
		rms/mean	0.0089	0.0065	0.0046	0.0035	0.0027
		CPU time (s)	2.67	7.66	19.25	35.05	60.46
1.0	DOM	rms	0.0017	0.0012	0.0009	0.0007	0.0008
	HYDRA	rms	0.0070	0.0030	0.0015	0.0009	0.0007
		rms/mean	0.0081	0.0034	0.0018	0.0011	0.0008
		CPU time (s)	0.76	2.22	5.56	11.61	23.03
10.0	DOM	rms	0.0023	0.0027	0.0029	0.0030	0.0031
	HYDRA	rms	0.0003	0.0015	0.0021	0.0024	0.0026
		rms/mean	0.0034	0.0146	0.0207	0.0240	0.0260
		CPU time (s)	0.18	0.54	1.45	3.18	6.30

This is consistent with the analytical solution given by Eq. (45) for a transparent medium, which yields

$$\frac{\mathrm{d}q^*(\tau)}{\mathrm{d}\tau} = \frac{\mathrm{d}q(\tau)/\mathrm{d}\tau}{\sigma(T_w^4 - T_{\mathrm{gas}}^4)} \approx -4E_2(0) = -4.00$$

If the medium emits and absorbs with $\tau_L = 0.1$, then $\mathrm{d}q/\mathrm{d}\tau$ is no longer constant, but it remains approximately constant, as shown in Fig. 3(a). The absolute value is greater as the distance from the walls decreases, as discussed above.

On the contrary, in the case of an optically thick medium, e.g., $\tau_L = 10.0$, the radiation emitted at a given point is rapidly absorbed. This means that the radiation intensity leaving the walls will have a marginal influence on the incident radiation, except in the close vicinity of the walls. Apart from this vicinity, the incident radiation will be approximately equal to $4\pi I_b$, because $I(\tau, \theta) \approx I_b$. This means that $\mathrm{d}q/\mathrm{d}\tau$ will be close to zero, as given by Eq. (43), and demonstrated by the results plotted in Fig. 3(c). Physically, this means that the radiation emitted by the medium at a given location is absorbed in its close vicinity, and therefore the radiative source is very small. This is no longer true when the distance from the walls is small, and this causes a sharp gradient of the radiative source close to the walls and a relatively large heat flux to the walls.

If the medium is neither optically thin nor optically thick, then the radiative heat source lies between those in the limiting cases of optically thin and optically thick media. Hence, there is a stronger variation of the radiative heat source along the domain compared with the optically thin case, but a smaller gradient close to the wall compared with the optically thick case.

The predicted normalized radiative heat source is shown in Fig. 3 along with the analytical solution as a function of the distance between the walls for different angular discretizations and optical thicknesses. The results were computed using a uniform grid with $N_x = 40$ control volumes. The errors are quantified in Table 1 by the root mean square (rms) defined as

$$\mathrm{rms}\left(\frac{\mathrm{d}q^*}{\mathrm{d}\tau}\right) = \frac{1}{N_x}\sqrt{\sum_{i=1}^{N_x}\left[\left(\frac{\mathrm{d}q^*}{\mathrm{d}\tau}\right)_{\mathrm{predicted}} - \left(\frac{\mathrm{d}q^*}{\mathrm{d}\tau}\right)_{\mathrm{analytical}}\right]^2} \quad (47)$$

and by the root mean square normalized by the mean value:

$$\frac{\mathrm{rms}\left(\frac{\mathrm{d}q^*}{\mathrm{d}\tau}\right)}{\frac{\mathrm{d}q^*}{\mathrm{d}\tau}} = \frac{\sqrt{\sum_{i=1}^{N_x}\left[\left(\frac{\mathrm{d}q^*}{\mathrm{d}\tau}\right)_{\mathrm{predicted}} - \left(\frac{\mathrm{d}q^*}{\mathrm{d}\tau}\right)_{\mathrm{analytical}}\right]^2}}{\sum_{i=1}^{N_x}\left(\frac{\mathrm{d}q^*}{\mathrm{d}\tau}\right)_{\mathrm{predicted}}} \quad (48)$$

Table 1 also shows the errors obtained using the discrete ordinates method using the same spatial and angular discretizations, along with the computational requirements. It can be seen that the discrete ordinates method yields smaller errors for an optically thin medium, but larger errors for an optically thick medium. The reported CPU time should be regarded as indicative since no effort was made to speed up the solution procedure using faster solvers that exploit the sparseness of the matrix of coefficients.

The rms of $\mathrm{d}q^*/\mathrm{d}\tau$, either normalized or not by the mean value, decreases with the increase of the number of control angle elements for both $\tau_L = 0.1$ and $\tau_L = 1.0$, as expected. However, a different behaviour is observed for $\tau_L = 10.0$. In this case, the errors increase when a finer angular discretization is employed. The reason for this may related to the interaction between the errors arising from the spatial and the angular discretization. This interaction occurs in the discrete ordinates and finite volume methods, as discussed in [14,21]. Briefly, the two error sources tend to compensate each other. This means that accurate solutions may be obtained even if the two errors are large provided that they are of the same magnitude, because their influence is opposite. If one of the error sources is eliminated, the accuracy of the numerical solution may decrease, because the other error source remains, and is no longer compensated.

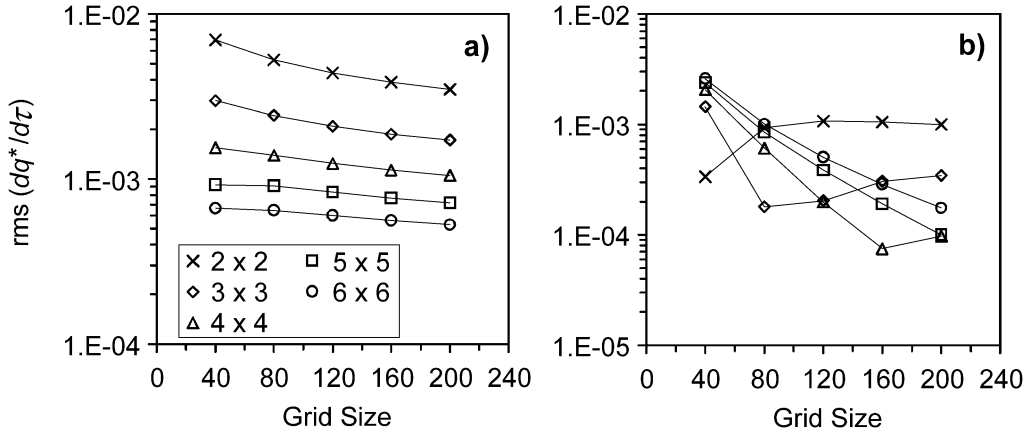

Fig. 4. Root mean square of the radiative heat source as a function of the angular and spatial discretizations. (a) $\tau_L = 1.0$; (b) $\tau_L = 10.0$.

In order to further investigate this issue, the rms of $dq^*/d\tau$ as a function of the grid size and angular refinement is shown in Fig. 4 for both $\tau_L = 1.0$ and $\tau_L = 10.0$. No anomalous behaviour occurs for $\tau_L = 1.0$. In this case, the increase of the number of control angle elements yields smaller errors for a given grid. Similarly, for a given number of control angle elements, the error decreases with grid refinement.

However, a different pattern is observed for $\tau_L = 10.0$. The angular refinement may yield larger errors for a given grid, if this grid is not fine enough. However, if the grid is fine enough, i.e., if the spatial discretization errors are small enough, then the angular refinement actually yields smaller errors, i.e., the angular discretization error decreases and the solution accuracy increases. Similarly, the grid refinement may yield larger errors for a given angular discretization if this discretization is not fine enough. However, for a fine enough angular discretization, i.e., for negligible angular discretization errors, grid refinement yields smaller errors, i.e., the spatial discretization error decreases and the solution accuracy increases.

The reduction of the spatial discretization error may be accomplished either by grid refinement or by a better distribution of the grid nodes. In the case of an optically thick medium, it has been observed that the radiative heat source exhibits a strong gradient in the vicinity of the walls, but remains approximately constant in a wide area far from the walls. Therefore, if a non-uniform grid is employed with the grid nodes concentrated near the wall, the solution accuracy is expected to improve. This is illustrated in Fig. 5 for $\tau_L = 10.0$. Several grids with a total of $N_x = 40$ grid nodes were used and distributed by means of an expansion factor that increases the size of the control volumes from the walls towards the symmetry plane. As this factor becomes larger, more concentrated are the grids nodes close to the walls. The results show that for the largest expansion factors, i.e., when the spatial discretization errors are small enough, the increase of the angular refinement yields a decrease of the solution error.

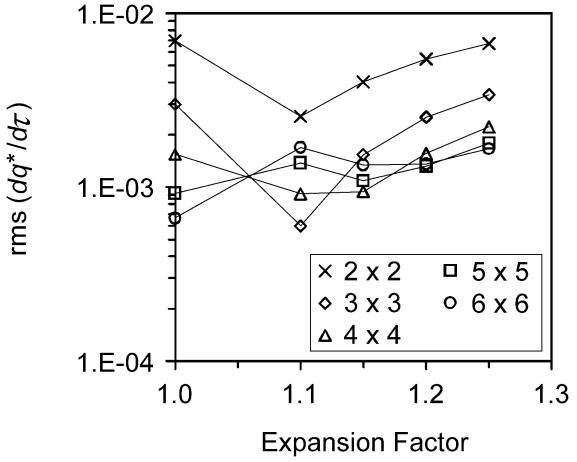

Fig. 5. Root mean square of the radiative heat source as a function of the expansion factor of the grid for several angular discretizations and for $\tau_L = 10.0$.

Table 2 shows the net heat flux on the walls normalized by the difference between the emissive power of the medium and the emissive power of the walls. The analytical solution is given by Eq. (44). The absolute, E, and the relative, η, errors are listed as a function of the angular refinement and optical thickness of the medium. A uniform grid with $N_x = 40$ control volumes was used. It can be seen that the exact solution is approached as the number of control angle elements increases, regardless of the optical thickness of the medium. The solution accuracy increases with the increase of the optical thickness of the medium.

Finally, the influence of the emissivity of the wall is investigated. The predictions were made for the same spatial grid, 4×4 control angle elements per octant and $\tau_L = 1.0$. If the emissivity of the wall increases, I_w is more influenced by the temperature of the wall, and decreases because $T_w < T_{\text{gas}}$. Therefore, the incident radiation decreases too, yielding an increase of the absolute value of the radiative heat source. The proposed method reproduces this behaviour and the predicted solution closely follows the analytical one, as shown in Fig. 6.

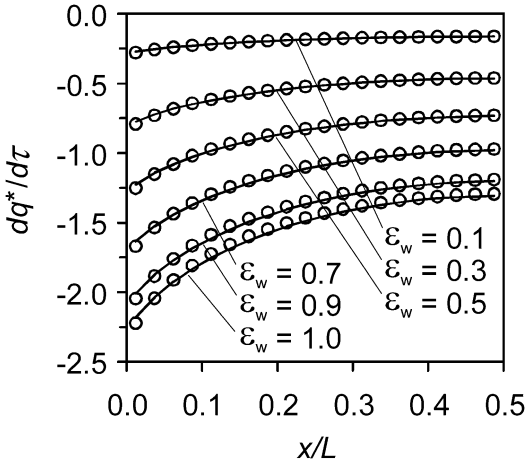

Fig. 6. Normalized radiative heat source as a function of the emissivity of the wall (solid lines: analytical solution; symbols: predictions).

Table 2
Net heat flux on the walls normalized by the difference between the emissive power of the medium and the emissive power of the walls as a function of the angular refinement and optical thickness of the medium

Optical thickness		Angular discretization ($N_\theta \times N_\varphi$ per octant) 2 × 2	3 × 3	4 × 4	5 × 5	6 × 6	Exact solution
0.1	Heat flux	0.1384	0.1398	0.1409	0.1416	0.1421	0.1434
	E	0.0050	0.0036	0.0025	0.0018	0.0013	
	η	0.0349	0.0251	0.0174	0.0126	0.0091	
1.0	Heat flux	0.4274	0.4342	0.4361	0.4367	0.4369	0.4384
	E	0.0110	0.0042	0.0023	0.0017	0.0015	
	η	0.0251	0.0096	0.0052	0.0039	0.0034	
10.0	Heat flux	0.4895	0.4963	0.4983	0.4990	0.4994	0.5000
	E	0.0105	0.0037	0.0017	0.0010	0.0006	
	η	0.0210	0.0074	0.0034	0.0020	0.0012	

Further insight into the solution accuracy is provided by the rms of $\mathrm{d}q^*/\mathrm{d}\tau$, which is given in Table 3. It shows that the rms is smaller for highly reflecting boundary surfaces. However, this is mainly due to the smaller values of the radiative heat source. In fact, the rms normalized by the mean value of $\mathrm{d}q^*/\mathrm{d}\tau$ is approximately constant, i.e., the solution accuracy is approximately independent of the emissivity of the walls.

The net heat flux on the walls is given in Table 4. The net heat flux increases with the increase of the emissivity of the walls. The error of the predicted heat flux also increases with the increase of the emissivity of the walls, but it remains lower than 1%.

Isotropically scattering medium. In this problem, a plane medium with isotropic scattering is studied. The medium neither absorbs nor emits. Since the medium is grey, this problem is mathematically equivalent to that of an emitting-absorbing and non-scattering medium in radiative equilibrium. The walls may be either grey or black and are maintained at prescribed temperature. This problem has been originally solved by Heaslet and Warming [22], and is addressed in detail in [20].

Table 3
Root mean square of the radiative heat source normalized by the difference between the emissive power of the medium and the emissive power of the walls as a function of the emissivity of the walls

	Emissivity of the walls 0.1	0.3	0.5	0.7	0.9	1.0
rms	0.0003	0.0009	0.0015	0.0022	0.0029	0.0026
rms/mean	0.0017	0.0017	0.0018	0.0019	0.0020	0.0017

Table 4
Net heat flux on the walls normalized by the difference between the emissive power of the medium and the emissive power of the walls as a function of the emissivity of the walls

	Emissivity of the walls 0.1	0.3	0.5	0.7	0.9	1.0
Predicted heat flux	0.0972	0.2757	0.4361	0.5808	0.7121	0.7733
Exact heat flux	0.0973	0.2767	0.4384	0.5849	0.7183	0.7806
E	0.0001	0.0010	0.0023	0.0041	0.0062	0.0073
η	0.0012	0.0036	0.0052	0.0070	0.0086	0.0094

A non-dimensional temperature field, $\phi(\tau)$, and a non-dimensional radiative heat flux, ψ, may be defined as

$$\phi(\tau) = \frac{T^4(\tau) - T_{w,2}^4}{T_{w,1}^4 - T_{w,2}^4} = \frac{\phi_b(\tau) + (1/\varepsilon_2 - 1)\psi_b}{1 + \psi_b(1/\varepsilon_1 + 1/\varepsilon_2 - 2)} \tag{49}$$

$$\psi = \frac{q}{\sigma(T_{w,1}^4 - T_{w,2}^4)} = \frac{\psi_b}{1 + \psi_b(1/\varepsilon_1 + 1/\varepsilon_2 - 2)} \tag{50}$$

where the indices 1 and 2 refer to the walls. Notice that the radiative heat flux does not vary across the medium for this problem. In the case of black walls, $\phi(\tau) = \phi_b(\tau)$ and $\psi = \psi_b$. These quantities are obtained from the numerical solution of the following integral equations:

$$\phi_b(\tau) = \frac{1}{2}\left[E_2(\tau) + \int_0^{\tau_L} \phi_b(\tau') E_1\big(|\tau - \tau'|\big)\,\mathrm{d}\tau'\right] \tag{51}$$

$$\psi_b = 1 - 2\int_0^{\tau_L} \phi_b(\tau') E_2(\tau')\,\mathrm{d}\tau' \tag{52}$$

Both $\phi_b(\tau)$ and ψ_b are independent of the emissivity and temperature of the walls. Moreover, $\phi(\tau)$ and ψ are independent of the temperature of the walls, although they are a function of the emissivity of the walls.

The predicted temperature field $\phi(\tau)$ as a function of the distance between the walls is given in Fig. 7 for three different cases: $\varepsilon_{w1} = 0.8$ and $\varepsilon_{w2} = 0.1$; $\varepsilon_{w1} = 0.8$ and $\varepsilon_{w2} = 0.5$; $\varepsilon_{w1} = 0.8$ and $\varepsilon_{w2} = 1.0$. The calculations were performed using a uniform grid with 20 control volumes (except for $\tau_L = 5.0$ where 100 control volumes were employed) and 5×5 control angle elements per octant. It can be seen that the gradient of the temperature profile becomes

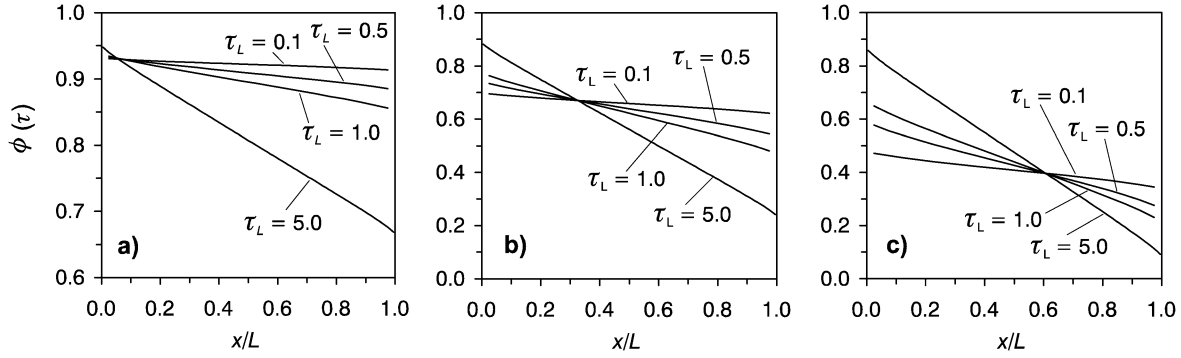

Fig. 7. Predicted normalized temperature field, $\phi(\tau)$, as a function of the distance between the walls. (a) $\varepsilon_{w1} = 0.8, \varepsilon_{w2} = 0.1$; (b) $\varepsilon_{w1} = 0.8, \varepsilon_{w2} = 0.5$; (c) $\varepsilon_{w1} = 0.8, \varepsilon_{w2} = 1.0$.

increasingly smaller as the optical thickness of the medium decreases. In the limit of a transparent medium, the temperature of the medium would be constant and $\phi_b = 0.5$, while in the limit of $\tau_L \to \infty$, the non-dimensional temperature would decrease from 1.0 at $x = 0$ to 0 at $x = L$.

The accuracy of the predictions is examined in Figs. 8 and 9, which show ψ_b and ψ for the three combinations of wall emissivities mentioned above, as a function of the optical thickness of the medium and angular discretization. A uniform grid with 20 control volumes was used. The horizontal lines show the exact fluxes. Apart from $\tau_L = 5.0$, refinement of the angular discretization improves the solution accuracy, i.e., the predicted heat flux converges to the exact one. However, if $\tau_L = 5.0$ the angular refinement does not yield more accurate results. This situation is similar to that observed in the first problem, suggesting that a finer spatial discretization is needed.

In fact, Fig. 10 reveals that an accurate solution requires both fine spatial and angular discretizations if $\tau_L = 5.0$. A fine grid along with a coarse angular discretization, or a coarse grid together with a fine angular discretization, do not give satisfactory results. In fact, a coarse grid and a coarse angular discretization may perform better, owing to the compensation between spatial and angular discretization errors. Both fine spatial and angular discretizations yield the most accurate solutions. This behaviour, which has been formerly reported for other solution methods [14,21], is independent of the emissivity of the walls, and occurs for optically thick media.

Table 5 shows a comparison between the one-dimensional radiative heat flux predicted by the present method and by the discrete ordinates method. The exact solution is also given. The same spatial and angular discretizations were employed for both methods. There is no clear trend regarding the most accurate method, although the proposed method appears to be more accurate for strongly scattering media, and the discrete ordinates method more accurate for weakly scattering media.

In the case of $\tau_L = 0.1$, the CPU time required to obtain the converged solution using a uniform grid with 20 control volumes, is equal to 0.43, 4.2 and 44.0 s for $2 \times 2, 5 \times 5$ and 10×10 control angle elements per octant, respectively.

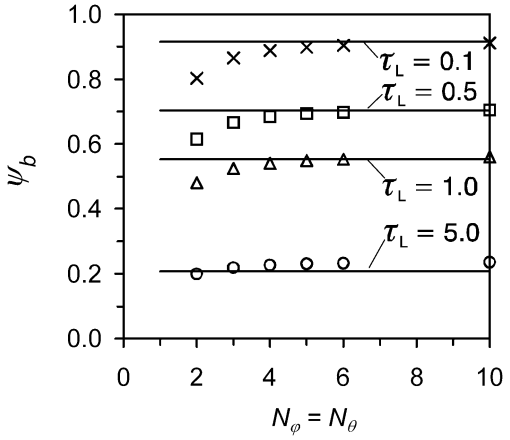

Fig. 8. Non-dimensional heat flux for black boundaries as a function of the angular discretization and optical thickness of the medium (solid lines: exact solution; symbols: predictions).

Table 5
Non-dimensional radiative heat flux for an isotropically scattering medium. The results for both the HYDRA and the discrete ordinates method were calculated using a uniform grid with 20 control volumes (except for $\tau_L = 5.0$ where 100 control volumes were employed) and 5×5 control angle elements per octant

ε_{w1}	ε_{w2}	τ_L	Exact	HYDRA	DOM
0.8	1.0	0.1	0.7451	0.7337	0.7445
		0.5	0.5986	0.5909	0.6006
		1.0	0.4860	0.4829	0.4926
		5.0	0.1975	0.1959	0.2026
0.8	0.5	0.1	0.4270	0.4232	0.4268
		0.5	0.3745	0.3714	0.3752
		1.0	0.3271	0.3257	0.3300
		5.0	0.1649	0.1638	0.1684
0.8	0.1	0.1	0.0967	0.0965	0.0967
		0.5	0.0937	0.0935	0.0938
		1.0	0.0904	0.0903	0.0907
		5.0	0.0711	0.0724	0.0718

The corresponding CPU time for $\tau_L = 5.0$ is 0.68, 9.2 and 127.7 s, respectively.

Anisotropically scattering medium. In the last problem, the medium scatters anisotropically with a constant scat-

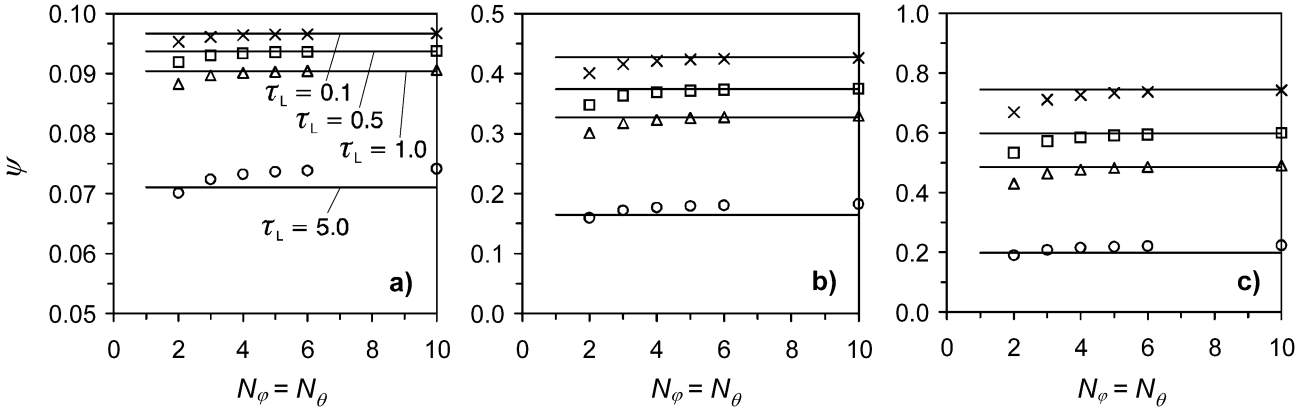

Fig. 9. Non-dimensional heat flux as a function of the angular discretization and optical thickness of the medium (solid lines: exact solution; symbols: predictions). (a) $\varepsilon_{w1} = 0.8, \varepsilon_{w2} = 0.1$; (b) $\varepsilon_{w1} = 0.8, \varepsilon_{w2} = 0.5$; (c) $\varepsilon_{w1} = 0.8, \varepsilon_{w2} = 1.0$.

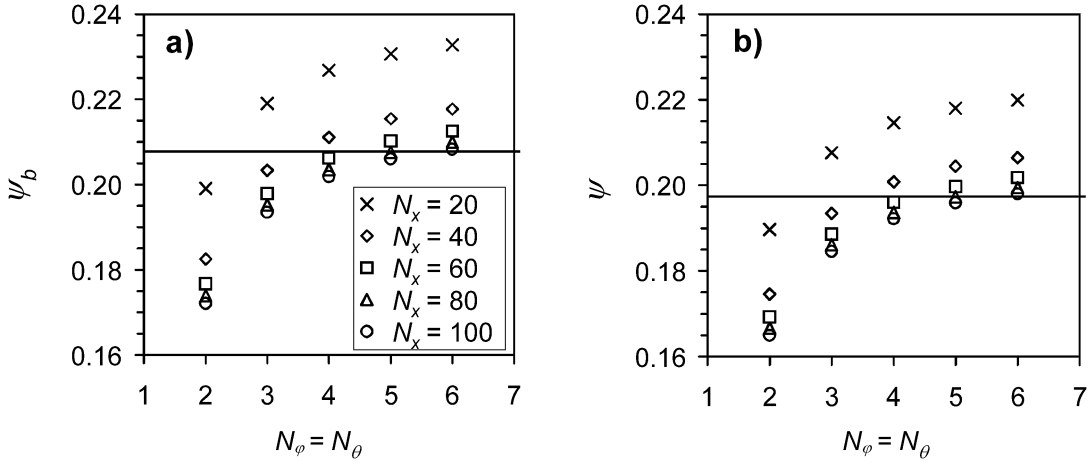

Fig. 10. Influence of the spatial and angular discretizations on the predicted non-dimensional heat flux for $\tau_L = 5.0$ (solid lines: exact solution; symbols: predictions). (a) Black boundaries; (b) $\varepsilon_{w1} = 0.8, \varepsilon_{w2} = 1.0$.

tering coefficient, but neither absorbs nor emits. A linearly anisotropic phase function is considered. The medium is in radiative equilibrium and confined between two black walls at different temperatures, $T_{w1} = 0$ and T_{w2}.

The incident heat flux on wall 2, normalized by the difference between the emissive powers of the walls, is plotted in Fig. 11 as a function of the optical thickness of the medium and the coefficient A_1 of the scattering phase function. The exact solution is taken from [23]. The incident heat flux increases with the optical thickness of the medium, i.e., with the scattering coefficient, but decreases if the anisotropy becomes more important. The predicted results were obtained using a uniform grid with 40 control volumes and 6×6 control angle elements per octant. They closely follow the reference solution [23], demonstrating the applicability of the present method to anisotropic scattering media.

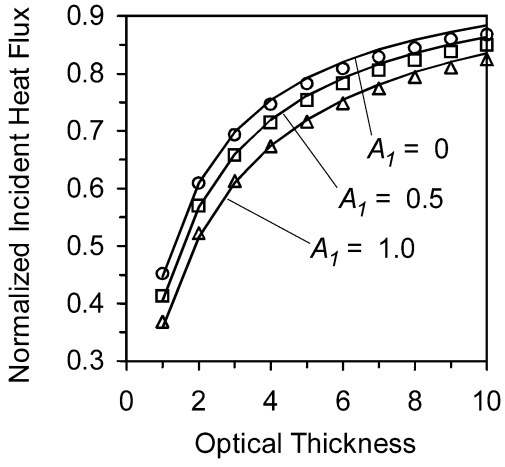

Fig. 11. Normalized incident heat flux on the hot wall as a function of the optical thickness of the medium for different linearly anisotropic scattering phase functions (solid lines: exact solution; symbols: predictions).

4. Conclusions

A new method for the solution of the radiative transfer equation has been presented and applied to one-dimensional grey media. The method assumes that the spatial and angular dependence can be split and the radiation intensity approximated as a linear combination of basis functions, dependent

only on the angular direction, with coefficients dependent only on the spatial coordinates. The finite volume method and the step scheme are used for spatial discretization, and the finite element method is used to define the basis functions used in the angular discretization. The method was applied to emitting, absorbing and scattering media. The influence of the spatial grid, angular discretization, optical thickness of the medium and emissivity of the walls was investigated. It was shown that the method works well and converges to the exact solution of the test problems for sufficiently fine spatial and angular discretizations. In the case of optically thick media, it was found that the solution accuracy may be adversely affected by refining either the angular discretization or the spatial discretization alone. It is necessary to refine simultaneously the spatial and angular discretizations to ensure a reduction of the solution error. The method is still in an initial stage of development, and therefore many important issues still need to be addressed. These include the implementation of more accurate spatial discretization schemes, an optimization of the solver, a more extensive comparison of the accuracy and computational requirements of the proposed method with other available methods, and the extension to complex enclosures and non-grey media.

Acknowledgements

This work was developed within the framework of project POCTI/EME/44107/2002, which is financially supported by FCT-Fundação para a Ciência e a Tecnologia under the programme POCTI (42.71% of the funds from FEDER and 57.29% from OE).

References

[1] H.C. Hottel, A.F. Sarofim, Radiative Transfer, McGraw-Hill, New York, 1967.
[2] J.R. Howell, Application of Monte Carlo to heat transfer problems, in: J.P. Hartnett, T. Irvine (Eds.), Advances in Heat Transfer, vol. 5, Academic Press, New York, 1968.
[3] M.P. Mengüç, R. Viskanta, Radiative transfer in three-dimensional rectangular enclosures containing inhomogeneous, anisotropically scattering media, J. Quant. Spectrosc. Radiat. Transfer 33 (1985) 533–549.
[4] Z. Tan, R. Howell, New numerical method for radiation heat transfer in nonhomogeneous participating media, J. Thermophys. Heat Transfer 4 (1990) 419–424.
[5] F.C. Lockwood, N.G. Shah, A new radiation solution method for incorporation in general combustion prediction procedures, in: 18th Symp. (Int.) on Combustion, The Combustion Institute, Pittsburgh, 1981, pp. 1405–1414.
[6] W.A. Fiveland, Discrete-ordinates solution of the radiative transport equation for rectangular enclosures, J. Heat Transfer 106 (1984) 699–706.
[7] G.D. Raithby, E.H. Chui, A finite-volume method for predicting a radiant heat transfer in enclosures with participating media, J. Heat Transfer 112 (1990) 415–423.
[8] J.C. Chai, H.S. Lee, S.V. Patankar, Ray effect and false scattering in the discrete ordinates method, Numer. Heat Transfer B Fundamentals 24 (1993) 373–389.
[9] J.P. Jessee, W.A. Fiveland, Bounded, high-resolution differencing schemes applied to the discrete ordinates method, J. Thermophys. Heat Transfer 11 (1997) 540–548.
[10] R. Koch, W. Krebs, S. Wittig, R. Viskanta, Discrete ordinates quadrature schemes for multidimensional radiative transfer, J. Quant. Spectrosc. Radiat. Transfer 53 (1995) 353–372.
[11] M.A. Ramankutty, A.L. Crosbie, Modified discrete ordinates solution of radiative transfer in two-dimensional rectangular enclosures, J. Quant. Spectrosc. Radiat. Transfer 57 (1997) 107–140.
[12] M. Sakami, A. Charette, Application of a modified discrete ordinates method to two-dimensional enclosures of irregular geometry, J. Quant. Spectrosc. Radiat. Transfer 64 (2000) 275–298.
[13] S.W. Baek, D.Y. Byun, S.J. Kang, The combined Monte-Carlo and finite-volume method for radiation in a two-dimensional irregular geometry, Internat. J. Heat Mass Transfer 43 (2000) 2337–2344.
[14] P.J. Coelho, The role of ray effects and false scattering on the accuracy of the standard and modified discrete ordinates method, J. Quant. Spectrosc. Radiat. Transfer 73 (2003) 231–238.
[15] W.A. Fiveland, J.P. Jessee, Finite element formulation of the discrete-ordinates method for multidimensional geometries, J. Thermophys. Heat Transfer 7 (3) (1994) 426–433.
[16] M.M. Razzaque, D.E. Klein, J.R. Howell, Finite element solution of radiative heat transfer in a two-dimensional rectangular enclosure with gray participating media, J. Heat Transfer 105 (4) (1983) 933–934.
[17] J.H. Joseph, W.J. Wiscombe, J.A. Weinman, The delta–Eddington approximation for radiative flux transfer, J. Atmospheric Sci. 33 (1976) 2452–2459.
[18] J.J. Dongarra, C.B. Moler, J.R. Bunch, G.W. Stewart, LINPACK User's Guide, Society for Industrial & Applied Mathematics, 1979.
[19] P.J. Coelho, A hybrid finite volume/finite element discretization method for the solution of the radiative transfer equation, in: 4th Int. Symposium on Radiative Transfer, Istanbul, Turkey, 18–25 June 2004.
[20] M.F. Modest, Radiative Heat Transfer, McGraw-Hill, New York, 1993.
[21] G.D. Raithby, Evaluation of discretization errors in finite-volume radiant heat transfer predictions, Numerical Heat Transfer B Fundamentals 36 (1999) 241–264.
[22] M. Heaslet, R. Warming, Radiative transfer and wall temperature slip in an absorbing planar medium, Internat. J. Heat Mass Transfer 8 (1965) 979–994.
[23] I.W. Busbridge, S.E. Orchard, Reflection and transmission of light by a thick atmosphere according to the phase function: $1 + x\cos\theta$, J. Astrophysics 149 (1967) 655–664.